The Effect of Out-of-Plane Loading on the Fracture of Aluminium 2024

M. Mostafavi, D.J. Smith, M.J. Pavier
Mechanical Engineering Department, University of Bristol, Bristol, U.K.

ABSTRACT

The effect of out of plane constraint on the fracture toughness of metals has long been appreciated. The extreme cases of out-of-plane constraint are typically held to be plane strain and plane stress: the stress intensity factor at fracture is lowest for thick (plane strain) specimens and greatest for thin (plane stress) specimens. However, situations that give higher levels of out-of-plane loading have rarely been considered, yet such conditions may occur in practical loading of cracked components. This combined numerical and experimental study explored the effects of applied out-of-plane loading on a cracked cruciform specimen tested in a biaxial test machine. It is observed that a stress intensity factor significantly below the plane strain fracture toughness can be measured at fracture when the applied out-of-plane load is sufficiently tensile.

1 INTRODUCTION

The specimen thickness effect on the fracture behaviour of metallic materials has always been an interesting area. Generally it is deemed that the fracture toughness decreases as thicker specimens are tested until the plane strain condition is met; thereafter the toughness is insensitive to the thickness. However, a stress field range wider than plane stress to plane strain is conceivable around the crack tip. Cracked structures may be loaded in such a way that higher or lower constraint levels than the plane strain or the plane stress conditions prevail. Take Fig. 1 for example, if the specimen is thick enough, representing the plane strain conditions, yet an out-of-plane tensile load is applied; the out-of-plane constraint becomes higher than the plane strain conditions. Similarly, if the specimen is very thin, i.e. plane stress, applying out-of-plane compressive load puts the specimen in conditions with lower out of plane constraint than the plane stress situation.

Although thickness effects have been extensively investigated in the past, studies on conditions higher or lower than plane strain or plane stress conditions respectively are scarce[1]. Occasionally five-point-bend (FPB) tests on shallow cracked cruciform specimens were conducted to investigate the effects of tensile out-of-plane loading. A number of studies resulted in decreasing the stress intensity factor upon fracture due to out-of-plane loading (e.g. [2-4]) while a few others did not show any effect (e.g. [5, 6]).

Because most of the experimental investigations were performed using the FPB cruciform specimens, shallow cracks had to be introduced in the specimens which leads to a mixed effect of shallow crack and the out-of-plane loading. In addition,

mostly semi-elliptical cracks were used where out-of-plane loading has influence on both out-of-plane and in-plane directions. Finally it should be mentioned that using bending specimens causes a varying stress field perpendicular to the crack front that increases the level of complexity and uncertainty of the obtained data and analyses. These ambiguities motivated the present study where long, straight cracks were introduced in specimens in the form of double edge notch tension configuration. The tests were carried out in a biaxial test machine to avoid complexities of the FPB tests. These tests provided a unique set of results in which the only changing parameter was the out-of-plane loading.

2 METHODLOGY

The out-of-plane loading effect is studied in the present work from three different points of view: macromechanical fracture behaviour, finite element, and micromechanics of the fracture surface. Each aspect is discussed below:

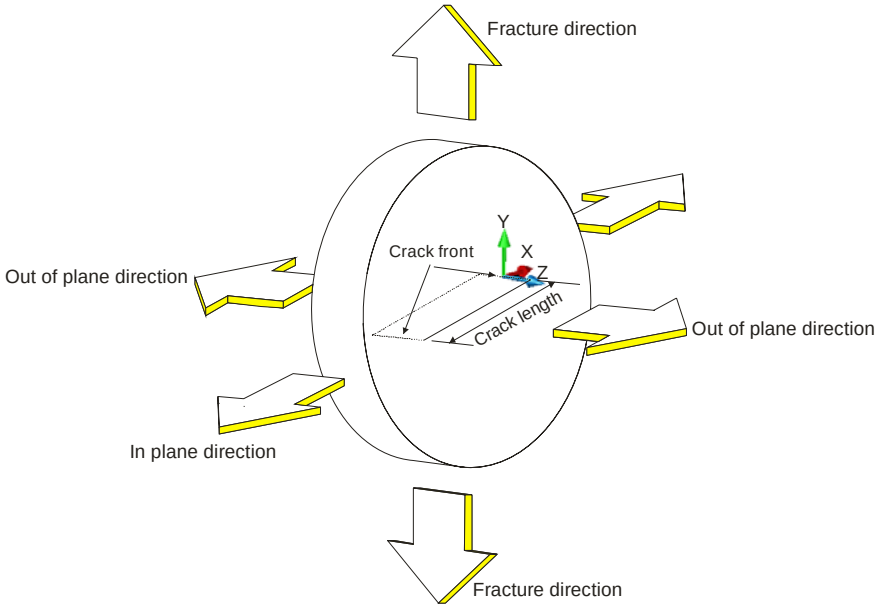

Fig. 1- Fracture, in-plane and out-of-plane directions in a cracked specimen

2.1 Macromechanical Effect

An especial specimen and appropriate grips were fabricated to perform tests in a biaxial test machine. The schematic specimen, grips and details of the crack is illustrated in Fig. 2; Fig. 3 shows the actual configuration of the test. The design was in a way that two side loading legs (in the Z direction) applied a constant load parallel to the crack fronts in a force control mode during the test. The other two loading legs (in the Y direction), perpendicular to the side load ones, ran in displacement control mode and applied a load on the specimen up to the point of failure.

As it can be seen in Fig. 2, the ligament in the specimen had four sides. To demonstrate that fracture initiates from the long edges, three specimens were considered. In the first specimen $2R = 4mm$ holes were drilled on the two short sides of EDM slot. The diameter of the EDM wire was 0.1mm. The rectangular shape ligament in the specimen then consisted of two long EDM cut edges and two blunt short edges. The second specimen experienced the same process except $2R = 2mm$ holes were drilled along the short edges. No holes were drilled in the third specimen ($R = 0mm$) which left a ligament with four 0.1mm EDM cut edges. Therefore, in case that the crack initiates from the short sides, the two drilled specimens which had blunt notches, should have shown elevated fracture load. It was observed that no meaningful difference exists between the nominal far field fracture load of these specimens and the specimen with the sharp EDM slot. Thus, it can be concluded that the crack initiates from the middle of the long EDM slot.

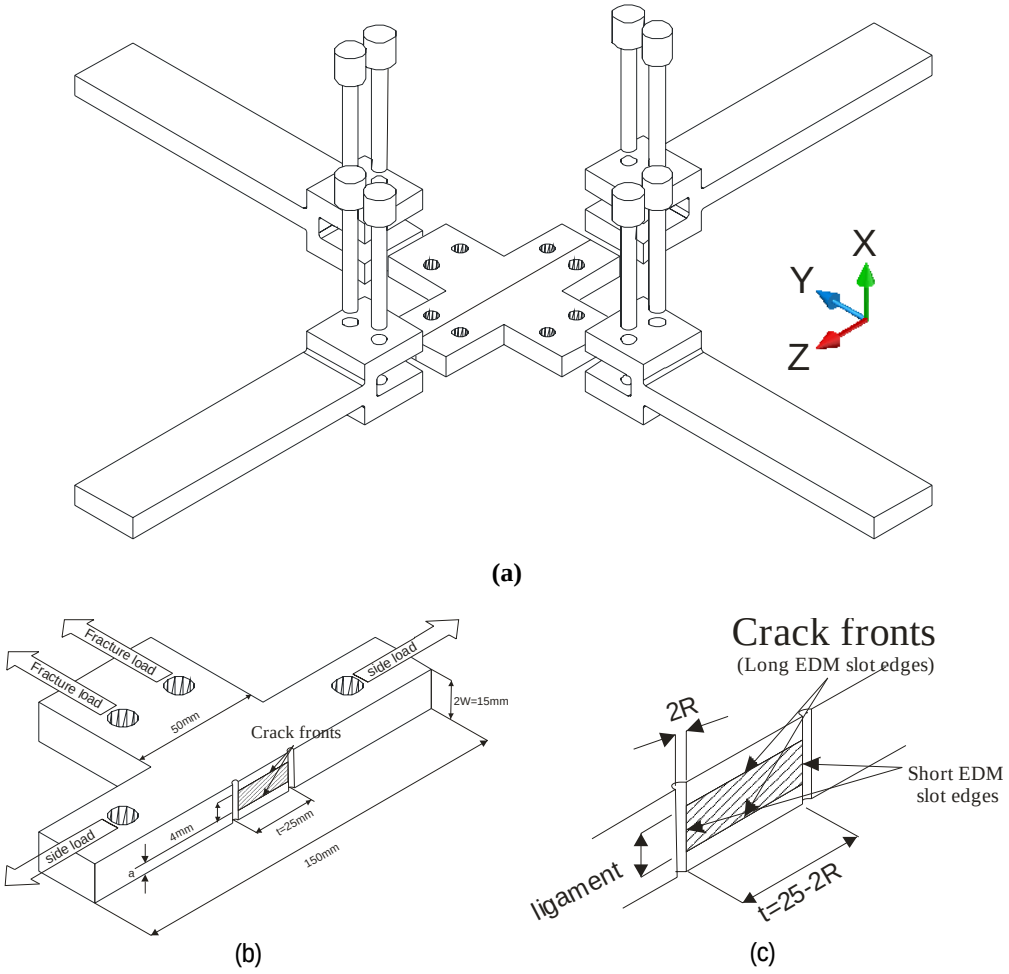

Fig. 2- Schematic view of test configuration (the hatched area is the uncracked ligament)

(a) overall test configuration (b) half of a biaxial specimen (c) details of the cracked area

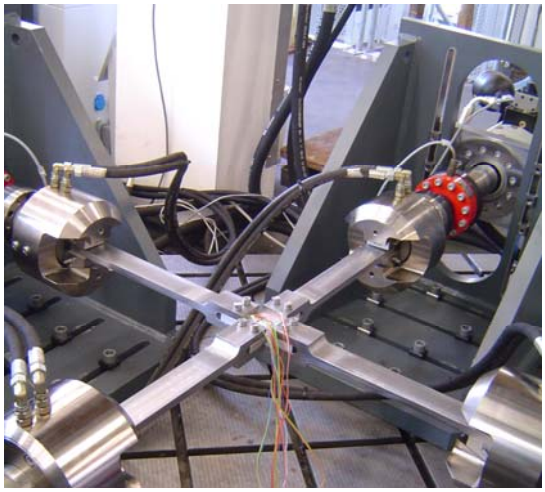

Fig. 3-Test setup

Loads of 0, 30, 60, 90kN were selected as out-of-plane loadings. Specimens were tested using a 100kN servo-hydraulic biaxial test machine. The load in the fracture direction was applied under displacement control with the rate of 0.1 mm/sec to maintain static fracture. All specimens demonstrated abrupt fracture which makes the fracture load $\tilde{F}_c$ detection straight forward. The details of the fracture loads can be observed in Fig. 4 in the form of the corrected fracture load F_c (Fig. 2), given by:

$$F_c = \tilde{F}_c \times \frac{t}{(t-2R)} \tag{1}$$

Table 1- Fracture toughness change in biaxial specimens

Side load F_T **(kN)**	**Corrected Fracture Load** $\tilde{F}_c$ **(kN)**	**Fracture Load** F_c **(kN)**	**Elastic-Plastic Toughness** J_c **(** $MPa.mm$ **)**	**Elastic J-integral** J_E **(** $MPa.mm$ **)**	J_c / J_E
0	45.20	55.12	18.14	14.38	1.26
0	56.05	60.92	18.50	13.95	1.32
0	58.84	58.84	18.74	13.93	1.34
30	54.60	54.60	15.44	12.29	1.25
60	50.91	50.91	13.22	10.98	1.20
60	50.73	50.73	13.10	10.90	1.20
90	46.72	46.72	10.88	9.39	1.16
90	46.00	46.00	10.72	9.27	1.16
90	49.90	49.90	12.97	10.83	1.20

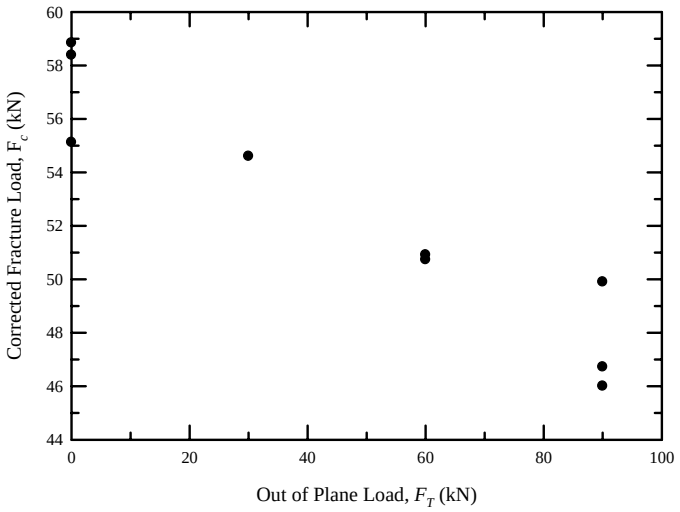

Fig. 4- Change in corrected fracture load vs. different side out-of-plane load

It can be seen in Table 1 that the specimens with no side loading show an average corrected fracture load of 58.29MPa. Applying maximum side load 90kN (higher out-of-plane constraint) decreases the fracture load up to 18% (47.54MPa). A smooth reduction curve is obtained when the side load increases (Fig. 4).

2.2 Finite Element Analysis

Finite element simulation of the test is carried out using the ABAQUS code. Considering the symmetry, just one eighth of the specimen is modelled (Fig. 5). A total number of 17,500 20-node brick elements were employed in a nonlinear elastic-plastic analysis. The tip of the crack was modelled as a 0.1mm diameter blunt notch like the real EDM slot. Material properties of Al2024 are reported in Table 2. Analyses were carried out in two steps. The first step was the preloading in side direction and the second step was applying the fracture load in the fracture direction. The *J*-integral was calculated automatically by ABAQUS using a domain integral method [7]. Elastic *J*-integral upon fracture J_E was calculated from an the elastic models and elastic-plastic *J*-integral upon fracture J_p from elastic-plastic models.

Table 2- Material properties of Al2024 (Isotropic hardening behaviour)

Modulus of elasticity (E)	71600MPa
Poisson's ratio (ν)	0.29
Yield stress (σ_y)	380MPa
Ultimate stress (σ_u)	450MPa
Plastic strain at ultimate stress (ε_u)	0.083

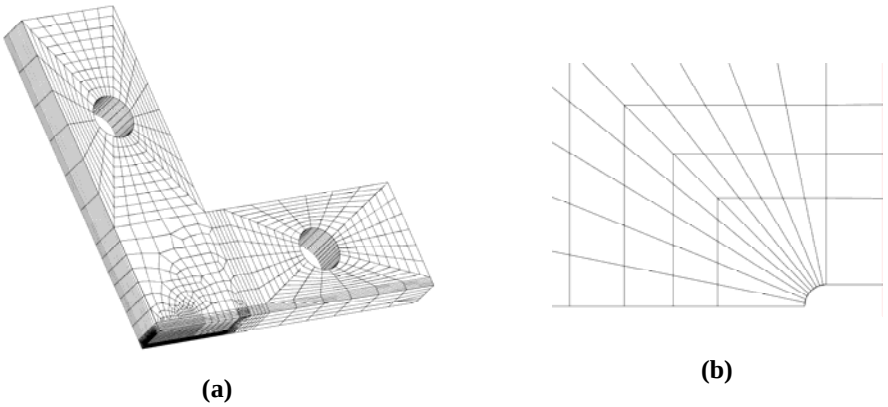

(a) **(b)**

Fig. 5- Finite element mesh (a) overview (b) crack tip

Because of the specimen shape and loading condition, a distribution of the *J*-integral is obtained along the crack front. Fig. 6 plots two samples of *J*-integral distribution with and without out-of-plane loading. Maximum value of the *J*-integral appeared in the middle of specimen that is reported in Table 1 as the representative value. This suggests that crack growth commences from the middle of the crack front. This confirms the experimental finding that shows the fracture load is insensitive to the shape of the ligament at its short edges which implies that the crack initiates from the long edges. It can be seen in Fig. 6 that the *J*-integral upon fracture drop due to out-of-plane loading is more dramatic than the decrease in the fracture load. A 37% decrease in the elastic-plastic *J*-integral upon fracture is observed.

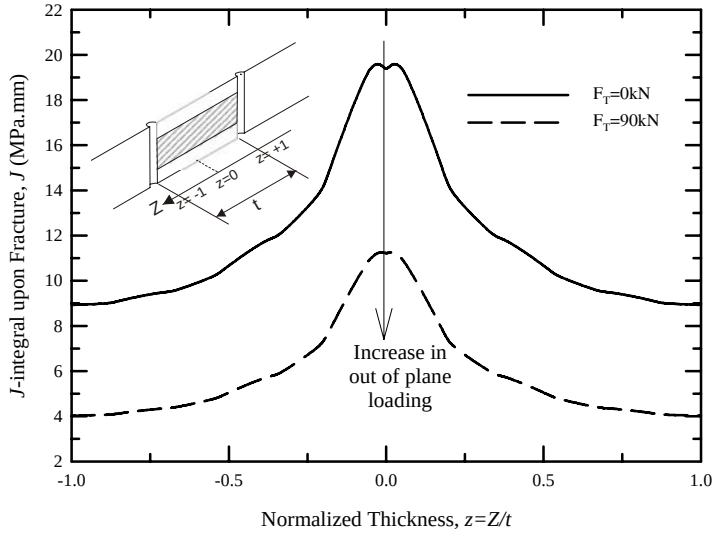

Fig. 6- J-integral distribution through crack front (J_c)

2.3 Micromechanical Effect

A Hitachi S-2300 scanning electron microscope was used to perform fractography on the specimens with different side loading. Because it is assumed that the crack initiates from the middle of the long EDM slot, all pictures were taken from that area, close to the original crack front. The interpretation of the fractographs will be discussed in the next section.

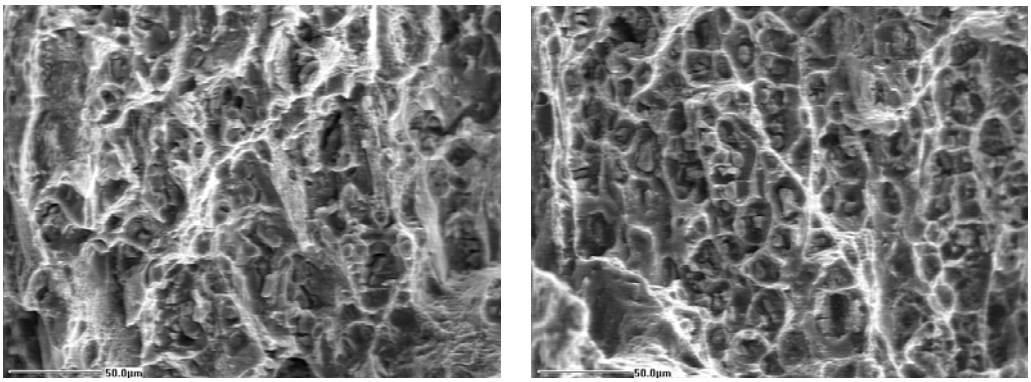

(a) **(b)**

Fig. 7- Fracture surface (a) no out-of-plane loading (b) 90kN out-of-plane loading

3 DISCUSSION

Although the two cases of plane strain and plane stress are usually discussed in the context of out-of-plane constraint, in practice higher or lower constraint levels are likely to happen. It is shown in the present paper that in case of constraints higher than the plane strain situation, the *J*-integral value upon fracture was less than the fracture toughness obtained from the standard tests. In the case of present study, when a 90kN force is applied on the biaxial specimens, roughly a 50% reduction is observed in the *J*-integral value upon fracture compared to *J*-integral upon fracture obtained from the standard test (i.e. fracture toughness).

Out of plane constraint can be measured by:

$$T_z = \frac{\sigma_{zz}}{\sigma_{xx} + \sigma_{yy}} \tag{2}$$

Fig. 8 shows the variation of *J*-integral upon fracture versus the out-of-plane constraint measure.

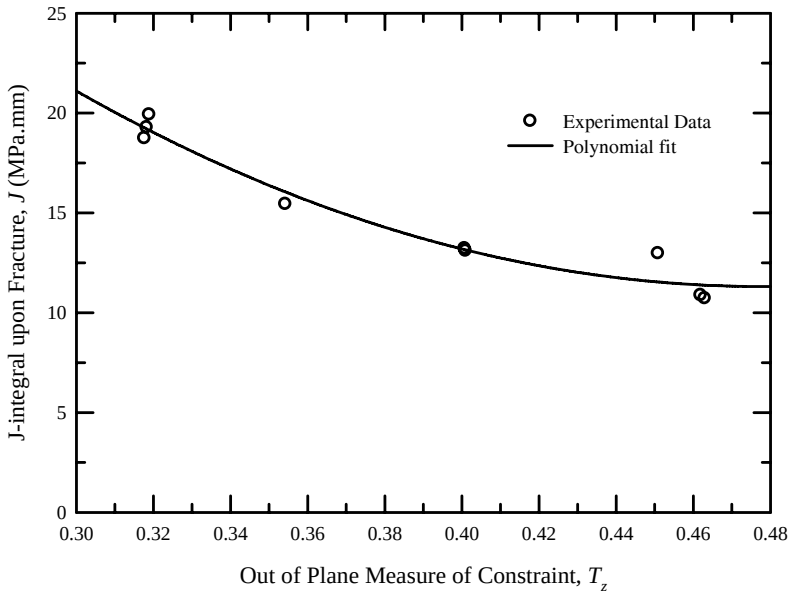

Fig. 8- Biaxial fracture toughness distribution against out-of-plane constraint measure

It can be observed in Table 1 that the ratio of the elastic plastic (J_c) *J*-integral to the elastic (J_E) values upon fracture is 1.3 at zero out-of-plane loading (i.e. plane strain condition). This difference decreases to 1.17 when maximum out-of-plane loading is applied (90kN). This effect was expected as out-of-plane loading results in less plasticity and material behaves in a more brittle manner. Also, the SEM pictures of the fracture surface of the biaxial specimens confirm the diminishing of the plastic deformation preceded by fracture. It can be seen in Fig. 7 that for a specimen with no out-of-plane loading, both tensile type, big, spherical voids and small, slipped shear type voids are observed in the fracture surface. However, the fracture surface of the specimen with maximum out-of-plane loading shows very limited shear type fracture regions which is the direct result of limiting the plasticity [8].

The decreasing trend of the $J - T_z$ gives rise to the question: if the standard fracture toughness is not the minimum value of the *J*-integral upon fracture How much is it and where does it take place? To answer these questions a set of triaxial tests seem to be appropriate, which is in the process of being conducted by the authors.

The effect of high out-of-plane loading has been discussed in this paper. Such effects can also be observed as a result of high in-plane loading. However, the high in-plane constraint or equivalently high *T*-stress can cause the crack propagation direction to deviate from its original direction which was not observed in this investigation. Change in the propagation direction is known as crack curving. Crack curving was recently discussed by Liu and Chao [9], they

showed that the crack curving can also lead to reduction in the *J*-integral upon fracture below the standard plane strain value.

Finally it is worth noting that this test has been conducted on Al2024 which is in the upper to lower shelf transition region at the room temperature. It is important to conduct similar tests on other materials (e.g. steel) and in different temperatures before a solid conclusion could be reached.

4 CONCLUSION

- A set of biaxial tests was conducted to investigate the effects of out-of-plane loading on the fracture behaviour of Al2024.

- It was observed that remarkable reduction in the fracture load of biaxially loaded specimens takes place due to high out-of-plane loading.

ACKNOWLEDGEMENTS

The financial sponsorship for this work provided by Engineering and Physical Sciences Research Council (EPSRC) of the UK government is gratefully acknowledged.

REFRENCES

1. Rudland, D.L., R. Mohan, N.D. Ghadiali, D. Detty, A.R. Rosenfield and G.M. Wilkowski, *The effect of constraint due to out-of-plane stress field on fracture of reactor pressure vessel steel- An experimental and numerical study*, in *Constraint effects in fracture - Theory and applications (ASTM STP 1244)*, M.T. Kirk and A. Bakker, Editors. 1995, ASTM: Philadelphia. p. 316-343.

2. McAfee, W., B.R. Bass and P.T. Williams, *Shallow flaws under biaxial loading conditions-Part I: the effect of specimen size on fracture toughness values obtained from large-scale cruciform specimens.* Journal of Pressure Vessel Technology, 2001. **123**: p. 10-24.

3. Pennell, W.E. and W.R. Corwin, *Reactor pressure vessel structural integrity research*. 1994, Oak Ridge National Laboratory, CONF-90410216--10.

4. Lidbury, D., *Validation of constraint based assessment methodology in structural integrity (VOCALIST)*. 2006, Serco Assurance.

5. Sattari-Far, I. and L. Dahlberg, *Fracture assessment of a brittle RPV under cold loading.* Nuclear Engineering and Design, 2004. **228**: p. 143-150.

6. Joyce, J.A., R.E. Link and J. Gaies, *Evaluation of the effect of biaxial loading on the T_o reference temperature using a cruciform specimen geometry*. Journal of ASTM International, 2005. **2**(1): p. 1-18.

7. ABAQUS, *User's Manual*. 2006: ABAQUS Inc., Prvidence, Rhode Island, Version 6.6.

8. Knott, J.F., *Private Communication*. 2008: Bristol.

9. Liu, S. and Y.J. Chao, *Variation of fracture toughness with constraint.* International Journal of Fracture, 2003. **124**: p. 113-117.